Received: 21 May 2024 | Revised: 3 October 2024 | Accepted: 4 October 2024

DOI: 10.1002/alz.14385

Alzheimer's & Dementia®
THE JOURNAL OF THE ALZHEIMER'S ASSOCIATION

RESEARCH ARTICLE

Elevated locus coeruleus metabolism provides resilience against cognitive decline in preclinical Alzheimer's disease

Elouise A. Koops[1] | Joyita Dutta[2] | Bernard J. Hanseeuw[3] | J. Alex Becker[3] | Maxime Van Egroo[1] | Prokopis C. Prokopiou[1] | Julie C. Price[1] | Steven E. Arnold[4] | Reisa A. Sperling[5,6] | Keith A. Johnson[3,5,6] | Heidi I. L. Jacobs[1,7] | for the Alzheimer's Disease Neuroimaging Initiative

[1]The Athinoula A. Martinos Center for Biomedical Imaging, Department of Radiology, Massachusetts General Hospital, Harvard Medical School, Boston, Massachusetts, USA

[2]Department of Biomedical Engineering, University of Massachusetts Amherst, Amherst, Massachusetts, USA

[3]Gordon Center for Medical Imaging, Department of Radiology, Massachusetts General Hospital, Harvard Medical School, Boston, Massachusetts, USA

[4]Alzheimer's Clinical and Translational Research Unit, Department of Neurology, Massachusetts General Hospital, Boston, Massachusetts, USA

[5]Department of Neurology, Massachusetts General Hospital, Boston, Massachusetts, USA

[6]Center for Alzheimer Research and Treatment, Department of Neurology, Brigham and Women's Hospital, Harvard Medical School, Boston, Massachusetts, USA

[7]Faculty of Health, Medicine and Life Sciences, Mental Health and Neuroscience Research Institute, Alzheimer Centre Limburg, Maastricht University, Maastricht, MD, The Netherlands

Correspondence
Heidi I.L. Jacobs, The Athinoula A. Martinos Center for Biomedical Imaging, Department of Radiology, Massachusetts General Hospital, Harvard Medical School, 149 13th Street, Charlestown, MA 02129, USA.
Email: hjacobs@mgh.harvard.edu

Data used in the preparation of this article were obtained from the Alzheimer's Disease Neuroimaging Initiative (ADNI) database (adni.loni.usc.edu). As such, the investigators within the ADNI contributed to the design and implementation of ADNI and/or provided data but did not participate in the analysis or writing of this report. A complete listing of ADNI investigators can be found at: http://adni.loni.usc.edu/wp-content/uploads/how_to_apply/ADNI_Acknowledgement_List.pdf

Funding information
Center for Functional Neuroimaging Technologies, Grant/Award Number: P41EB015896; Alzheimer's Association, Grant/Award Number: 23AARF-1026796;

Abstract

INTRODUCTION: Alterations in locus coeruleus' (LC) metabolic turnover are associated with Alzheimer's disease (AD)-pathology and cognitive impairment. However, the evolution of these changes across disease stages and their functional relevance remains unknown.

METHODS: We examined associations of [^{18}F]-fluorodeoxyglucose positron emission tomography (FDG-PET) -derived LC metabolism with clinical diagnostic status, cerebrospinal fluid (CSF) -based AD biomarkers of AD pathology, and cognitive decline in Alzheimer's Disease Neuroimaging Initiative (ADNI) participants ($n = 604$).

RESULTS: FDG-PET-derived LC metabolism was elevated in the earliest preclinical stages and lower in later disease stages. Higher LC metabolism was associated with attenuated memory decline in preclinical stages, particularly in those with low CSF $A\beta_{42,}$ but not in AD patients with cognitive impairment.

DISCUSSION: Higher locus coeruleus [^{18}F]-FDG-PET-derived signal in the early preclinical stages of AD can confer cognitive resilience and may reflect increased metabolic activity, whereas later stages are characterized by lower LC FDG-PET-derived signal, possibly due to neurodegeneration.

National Institutes of Health, Grant/Award Number: R21AG074220; National Institutes of Health Shared Instrumentation Grant Program, Grant/Award Number: S10RR023401

KEYWORDS
Alzheimer's Disease, biomarkers, cognitive decline, CSF, disease staging, FDG-PET, locus coeruleus, MRI, neuromodulatory subcortical systems, PET, preclinical

Highlights

- LC FDG-PET signal is lower in Alzheimer's disease (AD) patients.
- LC FDG-PET signal is higher in the preclinical stage of AD.
- We observed less memory decline in those with higher LC FDG-PET signal.
- Higher LC FDG-PET signal conferred cognitive resilience in preclinical AD.

1 | BACKGROUND

The neuropathologic hallmarks of Alzheimer's disease (AD) emerge decades prior to the onset of clinical symptoms and are characterized by the aggregation of extracellular beta-amyloid (Aβ) plaques and intracellular neurofibrillary tangles consisting of hyperphosphorylated tau.[1,2] Autopsy studies report that the locus coeruleus (LC) is among the earliest brain structures accumulating tau prior to any detectable pathology in the neocortex or the emergence of cognitive impairment.[1,3,4] Although tau accumulation within the LC starts early in adulthood, dendritic atrophy, loss of volume, and neuronal loss in the LC occur in subsequent later stages and are often associated with neurodegenerative disease.[4–7] In pursuit of effective therapies, the focus has shifted to detecting the earliest indicators of pathologic changes reflecting preclinical and even earlier stages of AD, where AD pathology is detectable but clinical symptoms are absent.[8] Whereas preclinical AD is characterized by in-vivo evidence of amyloidosis, autopsy studies indicated that tau pathology can emerge earlier in the LC, and physiologic LC changes may confer risk or resilience to preclinical AD.

The LC is the largest cluster of noradrenergic neurons in the central nervous system, providing the neuromodulator norepinephrine (NE) to large areas of the brain,[9,10] which modifies neuronal excitability and regulates brain energy metabolism.[11,12] Higher levels of NE metabolites have been related to cognitive impairment in both humans and animals.[13–17] Cerebrospinal fluid (CSF)-derived MHPG (3-methoxy-4-hydroxyphenyl-ethylene glycol) levels were higher in those with more severe cognitive impairment, and higher MHPG levels were associated with abnormal CSF Aβ and p-tau levels, cortical atrophy, faster cognitive decline and higher levels of neuropsychiatric symptoms in AD patients.[13,18,19] On the other hand, positron emission tomography (PET) studies of catecholamine synthesis in preclinical AD reported higher LC catecholamine synthesis with lower tau pathology and attenuated memory decline.[20,21] These findings suggest that higher NE metabolic turnover in preclinical disease stages may have a protective effect, whereas in later disease stages, higher NE metabolic turnover may accompany detrimental processes.[22] In support of this hypothesis, studies examining the LC's structural integrity and functional responsivity reported that higher LC integrity and activity corresponded to better memory function and preservation of cognitive abilities, even in the presence of high Aβ burden.[23,24]

Currently, the evolution of these elevations in NE-metabolites across the entire disease spectrum and their functional relevance remains unknown. Measuring LC metabolism in-vivo in a spatially informative manner would be valuable to the early detection of AD, given that these metabolic changes are presumed to occur prior to neurodegeneration. Dysregulation of NE synthesis and release across the different disease stages, as indicated by CSF and PET studies, implies that the energy demands of LC neurons may vary during the course of the disease since regulation of neurotransmission and glucose metabolism are coupled.[25] Energetic (glucose) demands can be measured in-vivo in humans using [^{18}F]fluorodeoxyglucose (FDG)-PET imaging. However, the size of the LC is smaller than the typical resolution or sensitivity of standard PET scanners, requiring dedicated post-processing frameworks incorporating MRI-derived anatomical information to recover PET resolution. Previous work showed that PET resolution can be recovered via deconvolution based on spatially-variant blur kernels that are stabilized using an MRI-based joint-entropy prior.[26] Leveraging this method, we aimed to investigate the relationship between FDG-PET-derived LC metabolism, clinical diagnostic status, and CSF-based biomarkers of AD pathology.

We hypothesized that the presence of underlying AD pathology in the preclinical stages and significant cell loss in the later stages of AD affect LC metabolism in a nonlinear manner, with higher LC metabolism in the preclinical stages and lower LC metabolism in the later stages of AD. In addition, to understand the functional implications of LC metabolism, we hypothesized that higher LC-derived FDG-PET signal would be associated with less cognitive decline, even in the context of AD pathology.

2 | METHODS

2.1 | Participants

Data used in the preparation of this article were obtained from the Alzheimer's Disease Neuroimaging Initiative (ADNI) database (adni.loni.usc.edu). We included 604 individuals from the ADNI-1 and

ADNI-2/GO cohorts with a structural 3T magnetic resonance imaging (MRI) scan, FDG-PET scan, and CSF-derived biomarker data at baseline (Table 1). Diagnostic groups were based on ADNI classification that was consistent over the ADNI-1/2/GO cohorts and grouped individuals into cognitively normal (CN), mild cognitive impairment (MCI), and AD. CN participants in the ADNI study showed no sign of cognitive impairment, dementia, or depression and had a Clinical Dementia Rating Scale (CDR) Sum of Boxes score of 0. Participants with MCI had preserved daily living activities and a CDR of 0.5. Education-adjusted Wechsler Memory Scale Logical Memory II derived scores and Mini-Mental State Examination (MMSE) scores were further used to define the MCI and AD groups. To be considered either control or MCI, participants needed to have an MMSE score between 24–30 (inclusive), whereas individuals in the AD group needed to have a CDR of 0.5 or 1 and MMSE scores between 20–26 (inclusive). In line with the ATN model of disease progression,[27] we further classified participants into disease-staging groups based on clinical status and biomarker evidence, resulting in a control group without cognitive impairment or biomarker positivity, a preclinical group with evidence of AD pathologic change, and a prodromal/AD group with evidence of AD pathologic change and a diagnostic grouping of MCI or dementia to investigate LC metabolism in the context of disease staging. AD pathologic change was derived from CSF beta-amyloid (A) and phosphorylated tau (T) levels. In line with ADNI standards, the cut-offs were defined as < 1100 pg/mL for amyloid positivity (Elecsys AD CSF assay (1-42; $A\beta_{42}$), Roche) and ≥ 27 pg/mL for tau positivity (Elecsys phosphorylated tau CSF assay [p-tau_{181}], Roche). Throughout this manuscript, we refer to the CN A+T- group as early preclinical and the CN A+T+ groups as late preclinical. *Apolipoprotein E (APOE)* status was determined for all participants. Participants suspected of non-AD pathologic change were excluded.

RESEARCH IN CONTEXT

1. **Systematic review**: The authors reviewed the literature using traditional (e.g., PubMed) sources. Despite knowledge of the early accumulation of Alzheimer's disease (AD) pathology in the locus coeruleus (LC) and the dysregulation of the noradrenergic system in later disease stages, little is known about LC metabolism in the earliest stages of AD, and its relationship to AD pathology, disease stage, and cognition. The relevant citations are appropriately cited.
2. **Interpretation**: Our findings point toward dysregulation of LC metabolism across AD disease stages, with elevated LC metabolism in the early preclinical stage conferring protective effects on memory function, even in the presence of elevated beta-amyloid ($A\beta$).
3. **Future directions**: Future work examining the relationship between LC metabolism and AD pathology progression will help to understand whether higher LC metabolism can no longer rescue memory function in later stages of the disease due to the increasing and spreading of AD pathology burden and neurodegeneration.

2.2 | Data processing

2.2.1 | Structural MRI

The anatomical T1-weighted scans were processed with the automated reconstruction protocol of FreeSurfer (FS, version 7.2.0). This protocol performs over 30 steps, including motion correction, Talairach registration, intensity normalization, skull-stripping, segmentation, and parcellation.[28] Pontine segmentation was performed using the FreeSurfer brainstem substructures segmentation tool, which uses a Bayesian algorithm relying on a probabilistic atlas of the brainstem,[29] to obtain the pontine region used as reference region for the FDG signal in sensitivity analyses. Reference regions (cerebellar white [CW], pons with the LC subtracted) and cortical regions used in control analyses were extracted from the FreeSurfer parcellated images in native space. The anatomical scans were registered to a Montreal Neurological Institute (MNI) template with Advanced Normalization Tools (ANTs) using bi-directional diffeomorphic registrations.[30] The inverse warps extracted from this transformation were applied to obtain the LC in native space by registering the MNI-based LC templates to each individual anatomical scan using nearest neighbor interpolation. LC metabolism was extracted from two LC masks, an in-house developed 7T magnetization transfer-weighted turbo flash (MT-TFL)-based mask[31] and an adapted Keren mask,[32] which was dilated and smoothed with a custom ellipsoid Gaussian kernel (σ = 1.12 superior-inferior axis, σ = 0.6 anterior-posterior) ensuring a smooth mask. FreeSurfer extracted fourth ventricle masks were subtracted from the dilated Keren mask to diminish the contribution of the CSF signal to the extracted LC FDG-PET signal. The 7T-based mask is constrained to the dorsal rostral part of the dilated and smoothed Keren mask, showing considerable overlap with the Keren mask (see Figure S1). This 7T MRI LC mask is a more constricted mask, which was created by delineation of voxels with a hyperintense signal on the study-specific MT-TFL template generated from iterative averaging of all intensity- and spatially-normalized individual MT-TFL images. Primary analyses were performed with the Keren mask and sensitivity analyses were performed using the 7T-based mask since the larger spatial extent of the Keren mask comprehensively includes the entire LC region (Figure 1). The Keren mask covers the caudal part of the LC, covering the LC in line with neuroanatomical knowledge as the mask was co-localized with *postmortem* evidence. Sensitivity analyses were performed with a shifted LC mask to determine the specificity of the results toward the LC. The LC mask was shifted toward the anterior pontine region (translation y-direction: 11 voxels, z-direction: -12 voxels; Figure S2).

TABLE 1 Sample characteristics and demographics.

Parameter	CN, $N = 240$[a]	MCI, $N = 252$[a]	AD, $N = 112$[a]	p-value[b]
Age	72.92 (5.90)	73.22 (7.34)	74.23 (8.31)	0.3
Sex				0.3
Female	115 (47.92%)	103 (40.87%)	49 (43.75%)	
Male	125 (52.08%)	149 (59.13%)	63 (56.25%)	
Biomarker group				**< 0.001**
A-T-	135 (56.25%)	0 (0.00%)	0 (0.00%)	
A+T-	75 (31.25%)	108 (42.86%)	0 (0.00%)	
A+T+	30 (12.50%)	144 (57.14%)	112 (100.00%)	
Education (years)	16.48 (2.64)	16.25 (2.65)	15.26 (2.79)	**< 0.001**
CSF p-tau$_{181}$ (pg/mL)	19.79 (7.49)	31.74 (16.80)	44.17 (14.87)	**< 0.001**
CSF Aβ_{42} (pg/mL)	1,194.35 (437.92)	705.90 (202.91)	597.15 (172.45)	**< 0.001**
MMSE	29.03 (1.18)	27.47 (1.85)	23.17 (1.99)	**< 0.001**
CDR Sum of Boxes				**< 0.001**
No impairment	240 (100.00%)	0 (0.00%)	0 (0.00%)	
Minor impairment	0 (0.00%)	213 (84.52%)	19 (16.96%)	
Very mild dementia	0 (0.00%)	36 (14.29%)	30 (26.79%)	
Mild dementia	0 (0.00%)	3 (1.19%)	62 (55.36%)	
Moderate dementia	0 (0.00%)	0 (0.00%)	1 (0.89%)	
LC metabolism (SUVr)	0.89 (0.11)	0.86 (0.12)	0.85 (0.11)	**0.008**
mPACC digit	−0.14 (2.81)	−7.14 (4.18)	−15.56 (3.18)	**< 0.001**

Note: Longitudinal cognition: CN $n = 107$, MCI $n = 181$, AD $n = 35$. Mean 2.4 (SD 1.4); range: 1–10 years.
Abbreviations: Aβ, beta-amyloid; AD, Alzheimer's Disease; CDR, Clinical Dementia Rating Scale; CN, control; CSF, cerebrospinal fluid; LC, locus coeruleus; MCI, mild cognitive impairment; MMSE, Mini-Mental State Examination; mPACC, modified Preclinical Alzheimer's Cognitive Composite; p-tau, phosphorylated tau; SUVr, standardized uptake value ratio.
[a]Mean (SD); *n* (%).
[b]One-way analysis of variance; Pearson's chi-squared test; Kruskal–Wallis rank sum test.

2.2.2 | PET imaging

Data were harmonized within the ADNI center (https://adni.loni.usc.edu/methods/pet-analysis-method/pet-analysis/). The harmonized FDG-PET preprocessing of ADNI included motion correction, averaging, standardizing, and intensity normalization using a participant-specific mask. We extracted the first available FDG-PET scan collected within 1 year of the baseline MRI. We registered these FDG-PET images to the T1 images using bi-directional diffeomorphic registrations in ANTs.[30] The FDG-PET signal was referenced to the CW tissue, as defined in Freesurfer. We performed secondary analyses referencing the FDG-PET signal to the pontine signal (excluding the LC) to investigate the impact of reference region on the results. To overcome the intrinsically limited spatial resolution of FDG-PET images, an in-house developed spatially-variant deconvolution stabilizing MR joint-entropy-penalized image deblurring algorithm[26] performing post-processing of reconstructed PET images was used to extract the FDG-PET signal within the LC and perform partial volume correction. This method was developed for the quantification of PET signals from small brain regions and was previously validated in a clinical neuroimaging study.[26] This anatomically guided PET image deblurring framework minimizes a composite cost function, which includes a data-fidelity term based on a spatially variant deconvolution model and a penalty term based on the joint entropy between the PET and the higher-resolution MR image. The cost function is minimized using the Limited-Memory Broyden-Fletcher-Goldfarb-Shanno (L-BFGS) optimization algorithm. The advantages of our information-theoretic approach compared to Geometric Transfer Matrix (GTM)-based methods are that it takes the spatial variability of resolution in PET into account, and it doesn't require precise segmentation of the anatomical image. These MATLAB-based scripts include proprietary information but are available upon request to Dr. Dutta. Low-resolution PET images had $1.5 \times 1.5 \times 1.5$ voxels with a $160 \times 160 \times 96$ grid size, and the super-resolved PET images had $1 \times 1 \times 1$ mm voxels with a $256 \times 256 \times 256$ grid size consistent with the corresponding anatomical MRI scans. To facilitate comparison with a previous report on LC FDG-metabolism in the ADNI cohort, we extracted the LC FDG-PET signal for the three diagnostic groups from the low-resolution FDG-PET images without deblurring and without applying the joint-entropy-prior-penalty algorithm. After the post-processing algorithm was applied to the FDG-PET scans, we further evaluated if we obtained expected results for the isthmus of the posterior cingulate, a cortical region robustly

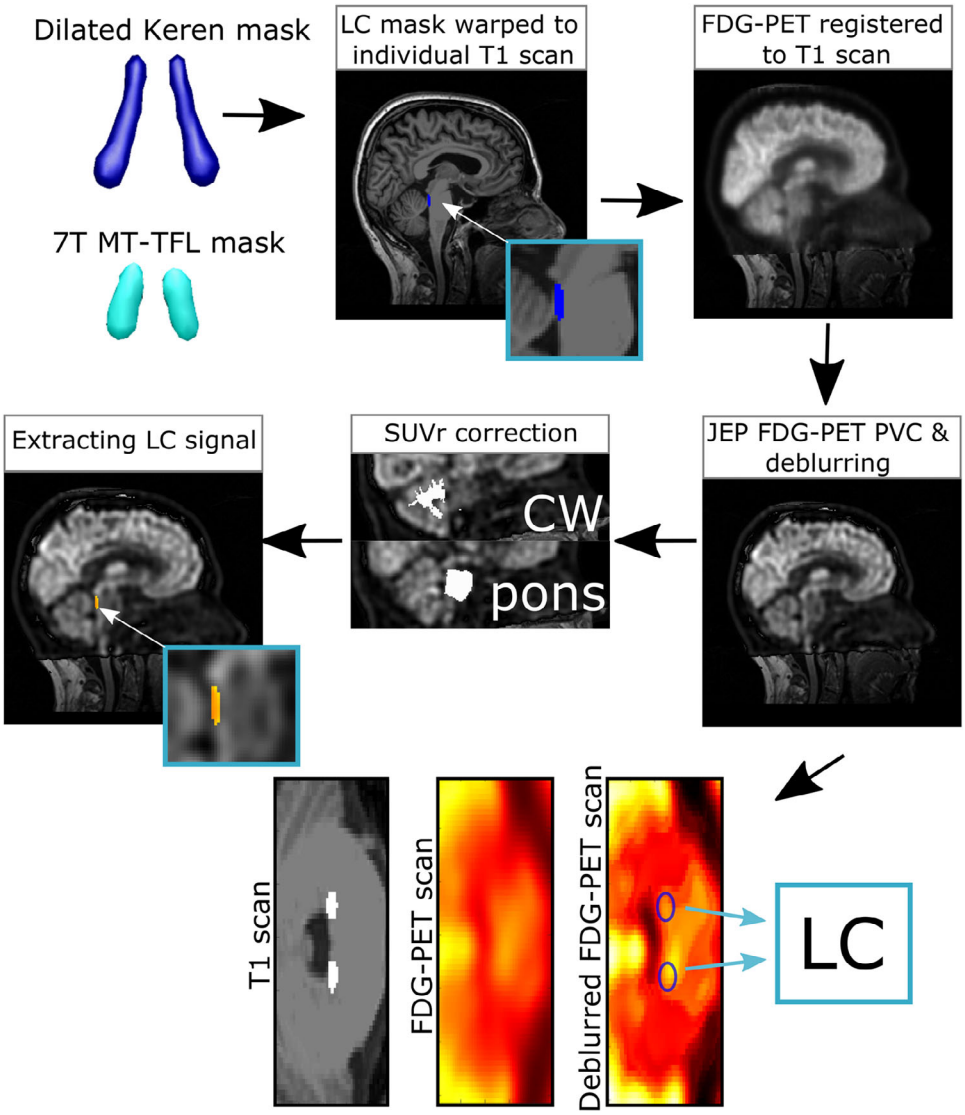

FIGURE 1 Processing pipeline to obtain deblurred and joint-entropy prior penalty corrected LC FDG-PET signal. (A) The primary analyses were performed using an LC template mask, based on the Keren template, which was dilated and smoothed with an ellipsoid Gaussian kernel to account for the low spatial resolution of PET scans and obtain a continuous mask. Sensitivity analyses were performed using an in-house developed LC mask based on 7 Tesla MT-TFL images. The processing consisted of the co-registration of the FreeSurfer-processed T1 anatomical images to an MNI template to facilitate the transformation of the MNI-based LC templates to native space. The FDG-PET images and LC templates were registered to native anatomic MRI space on an individual basis. The average signal from the LC was extracted after applying the MRI-PET joint entropy deblurring algorithm for the dilated Keren and 7T MT-TFL-based masks. FDG-PET images were referenced to either the CW matter or the pons (excluding the LC). CW, cerebellar white; FDG-PET, [18F]fluoredeoxyglucose positron emission tomography; LC, locus coeruleus; MNI, Montreal Neurological Institute; MRI, magnetic resonance imaging; MT-TFL, magnetization transfer-weighted turbo flash.

showing hypometabolism in AD, which is linked to neurodegeneration, pathology, and cognitive decline.[33–35]

2.3 | Cognition

The modified Preclinical Alzheimer's Cognitive Composite (mPACC) was used to investigate cognitive performance at baseline and over time. The mPACC is a standardized composite of the Delayed Recall portion of the Alzheimer's Disease Assessment Scale (ADAS), Logical Memory IIa Delayed Recall (LM), Digit Symbol Substitution Test (DSST), and MMSE. Scores were standardized by the baseline measurement derived mean and standard deviation of ADNI participants with normal cognition. Greater *z*-scores reflect better performance, and the sum of *z*-scores creates the composite. Additionally, the Harmonized Composite Scores of the Phenotype Harmonization Consortium (Alzheimer's Disease Sequencing Project [ADSP]) were used to investigate the association of LC FDG-PET signal and specific cognitive subdomains, including memory and executive function.[36] The composite memory score for ADNI incorporates the Weschler Memory Scale-Revised (WMS-R) Logical Memory Immediate and Delayed Recall, the MMSE, and the Montreal Cognitive Assessment (MoCA)

Immediate and Delayed recall items. The composite executive score for ADNI incorporates the Weschler Adult Intelligence Scale-Revised Digit Span Backward, Forward, and Digit Symbol elements, MMSE word spelling backward and letter elements, MoCA Abstraction, Trials, list of letters, Digits Backward and Forward, and Trails A and B time to complete. The included cognitive measures show high intercorrelations (composite memory scores–mPACC: $r = 0.93$, composite memory score–composite executive function: $r = 0.70$, composite executive function–mPACC: $r = 0.74$). We included longitudinal measurements for the cognitive composites and mPACC scores, resulting in data for $n = 604$ individuals with baseline data and $n = 323$ individuals with subsequent follow-up measurements spaced 12 months apart (Table S1).

2.4 | Statistical analysis

Statistical analyses were performed using RStudio (R version 4.2.2). Analysis of covariance (ANCOVA), followed by pairwise t-tests with Tukey-adjustment, correcting for multiple comparisons, was used to compare clinical groups on the demographic and biomarker variables, including the covariates of age and sex. The threshold for statistical significance was set at a two-sided $\alpha = 0.05$. Associations between LC FDG-PET signal and demographics were tested with linear regression models. To test our first hypothesis and investigate if the LC FDG-PET signal changes nonlinearly across disease stages, we used ANCOVA to investigate diagnostic and disease-stage-based group differences in the LC FDG-PET signal. Post hoc Tukey contrasts were applied in subsequent pairwise analyses, and age and sex were included as covariates. Linear regression models were used to investigate the relationship between LC FDG-PET signal and continuous values of CSF-based markers of phosphorylated tau and Aβ as well as cognitive performance at baseline in the entire group and within each diagnostic group. We used a robust linear regression with the Huber-M estimator for models with outliers.

We used the Benjamini—Hochberg[37,38] false-discovery rate (FDR) adaptive step-up procedure to correct for multiple comparisons for the cognitive tests. This method controls the FDR at a set alpha level for positive dependent test statistics. We implemented this method with the 'mutoss' package in R. Since the cognitive tests are highly overlapping and correlate highly ($r = 0.93$ (composite memory scores vs. mPACC), $r = 0.7$ (composite memory scores vs. composite executive function), $r = 0.74$ (composite executive function vs. mPACC), we will indicate if p-values are within critical p-values at $q = 0.05^{**}$ and $q = 0.1^{*}$. We performed this adaptive step-up procedure for tests performed on the same subset of data (e.g., within the CN group), which corresponds to critical p-values of 0.0167, 0.033, 0.05 at $q = 0.05$, and 0.033, 0.067, 0.1 at $q = 0.1$.

To test our second hypothesis, that LC FDG-PET signal is differently associated with cognitive performance across disease stages, we performed linear mixed-effects models (random intercept for each participant and random slope for time) with baseline LC FDG-PET signal as the predictor and changes in cognitive performance over subsequent visits as outcome variables in the entire group and within the diagnostic and disease-stage groups. We further interacted baseline LC FDG-PET signal with baseline CSF Aβ_{42} levels to examine whether changes in cognitive measurements across the entire group and the disease stage groups varied as a function of Aβ. To determine the best-fitting model, we compared the Akaike Information Criterion between models with a random intercept and slope to a model with only a random intercept. All models were corrected for age and sex, with the addition of years of education for the models investigating cognitive measurements. Johnson–Neyman analyses were performed to determine the range of CSF Aβ_{42} where LC metabolism was significantly associated with the outcome measure. Control analyses were performed by evaluating the outcomes for the isthmus of the posterior cingulate, a brain area with well-documented associations with AD pathology. Sensitivity analyses were performed with a shifted LC mask to determine the specificity of the results to the LC. We ran an additional analysis on the non-deblurred FDG-PET images to facilitate comparison with a previous report on FDG-metabolism in the ADNI cohort using ANCOVA followed by pairwise t-tests with Tukey-adjustment comparing the three diagnostic groups.

3 | RESULTS

3.1 | Basic characteristics

We included 604 participants from the ADNI-1 and ADNI-2/GO cohorts ($n = 240$ control, 252 MCI, and 112 AD; Table 1). The study sample had an age range from 55 to 91.4 years of age at baseline (mean ± SD = 73.3 ± 7), 45% of the sample was female, the average education level was 16.1 ± 2.7 years, and 53% carried at least one *APOE* ε4 allele. Older individuals had lower LC FDG-PET signal (β = -0.004, $t(599)$ = -6.45, $p < 0.0001$; Figure 2A), whereas LC FDG-PET signal was higher in females (β = -0.02, $t(599) = -2.22$, $p = 0.027$; Figure 2B). There was no association with education level ($\beta = 0.001$, $t(599) = 0.58$, $p = 0.56$), and no significant difference between *APOE* ε4 allele carriers and noncarriers ($\beta = 0.0121$, $t(599) = -1.29$, $p = 0.197$).

3.2 | LC metabolism in diagnostic and disease-staging groups

First, we observed differences in LC FDG-PET signal across diagnostic groups ($\beta = 0.099$, $F(2,596) = 4.06$, $p = 0.018$). Post hoc Tukey-adjusted pairwise contrasts indicated lower LC metabolism in individuals in the AD group compared to the control group ($\beta = 0.033$, $t = 2.61$, $p = 0.025$; Figure 2C and Table S2). Intersecting the diagnostic groups with the biomarker information revealed significant differences in LC FDG-PET signal across disease staging groups (β = 0.166, $F(2,596)$ = 6.86, p = 0.001; Figure 2D). Post hoc Tukey-adjusted pairwise contrasts showed that asymptomatic A+T-/A+T+ individuals (preclinical group) had higher LC FDG-PET signal compared to the asymptomatic A-T- individuals (control group; β = -0.004, t = -2.55, p = 0.0293).

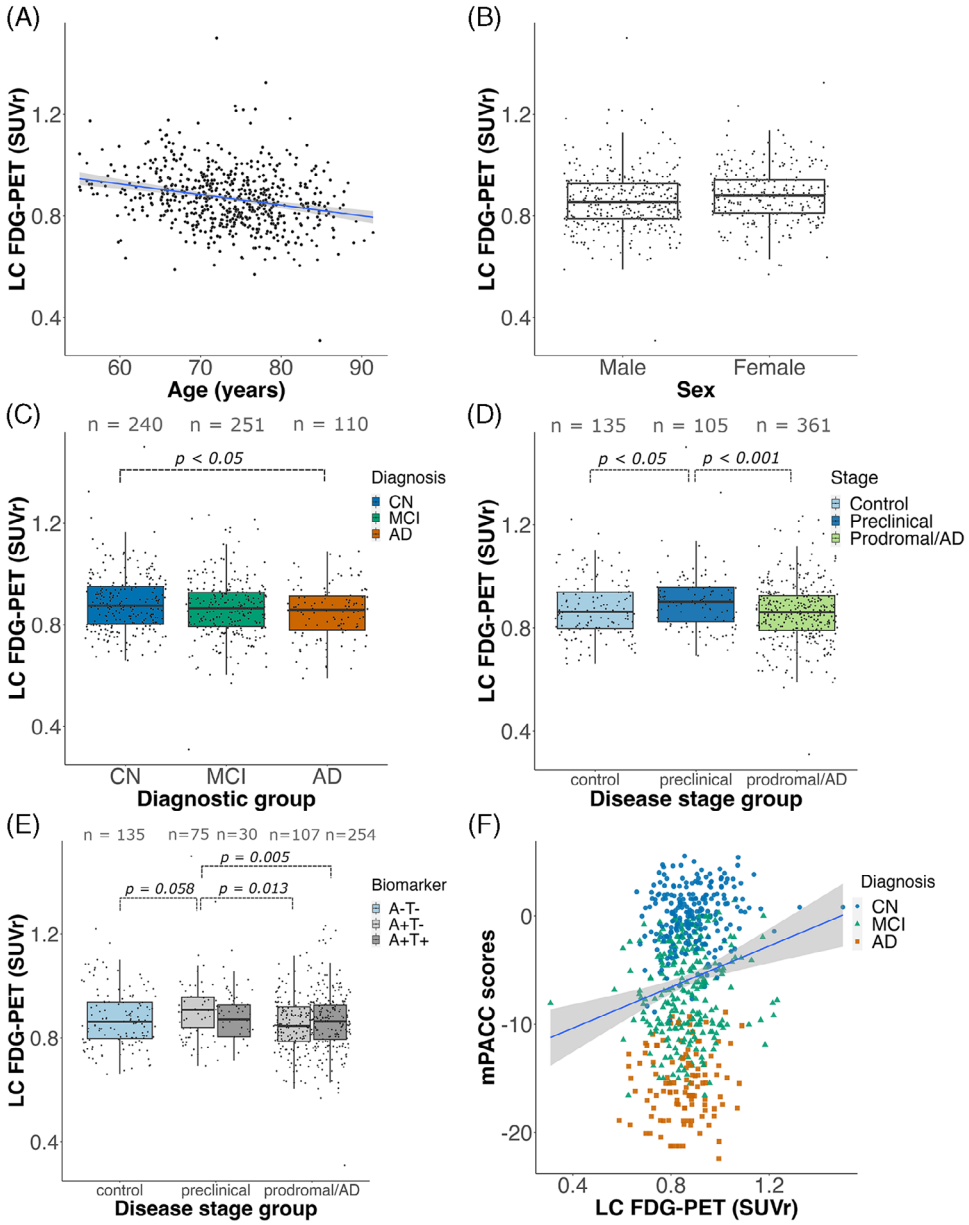

FIGURE 2 Associations between LC FDG-PET signal, sample characteristics, and diagnostic and disease stage groups. (A) A scatterplot with a regression line shows the relationship between the LC FDG-PET signal and age. FDG-PET-derived LC glucose metabolism was associated with age, with a lower LC signal in older individuals (B) Boxplot showing the relationship of LC FDG-PET signal and sex. LC FDG-PET signal was higher in females than in males. (C) Boxplot showing LC FDG-PET signal per diagnostic group. The AD group showed significantly lower LC metabolism compared to the control group. (D) Boxplot showing LC FDG-PET signal per disease stage group. The preclinical group showed significantly higher LC FDG-PET signal compared to both the control and the prodromal/AD groups. (E) Boxplot splitting the preclinical group and prodromal/AD group according to biomarker status, showing the increase in LC FDG-PET signal is primarily driven by the early preclinical (CN A+T-) group. (F) A scatterplot with a regression line (entire sample) shows the association between FDG-PET-derived LC signal and mPACC scores, with lower LC signal corresponding to worse mPACC scores. A+T-, amyloid positive and tau negative; A+T+, amyloid and tau positive; AD, Alzheimer's disease; A-T-, amyloid and tau negative; CN, cognitively normal; FDG-PET, [18F]fluorodeoxyglucose positron emission tomography; LC, locus coeruleus; MCI, mild cognitive impairment; mPACC, modified Preclinical Alzheimer's Cognitive Composite; SUVr, standardized uptake values referenced to the cerebellar white.

Similarly, the LC FDG-PET signal of the preclinical group was higher than that of the prodromal/AD group consisting of individuals with cognitive impairment and biomarker positivity (β = 0.045, t = 3.7, p = < 0.001). No differences were observed between the prodromal/AD and control groups (β = 0.009, t = 0.78, p = 0.714). Further exploration showed that within the preclinical group, this effect was most pronounced for A+T- individuals (Figure 2E).

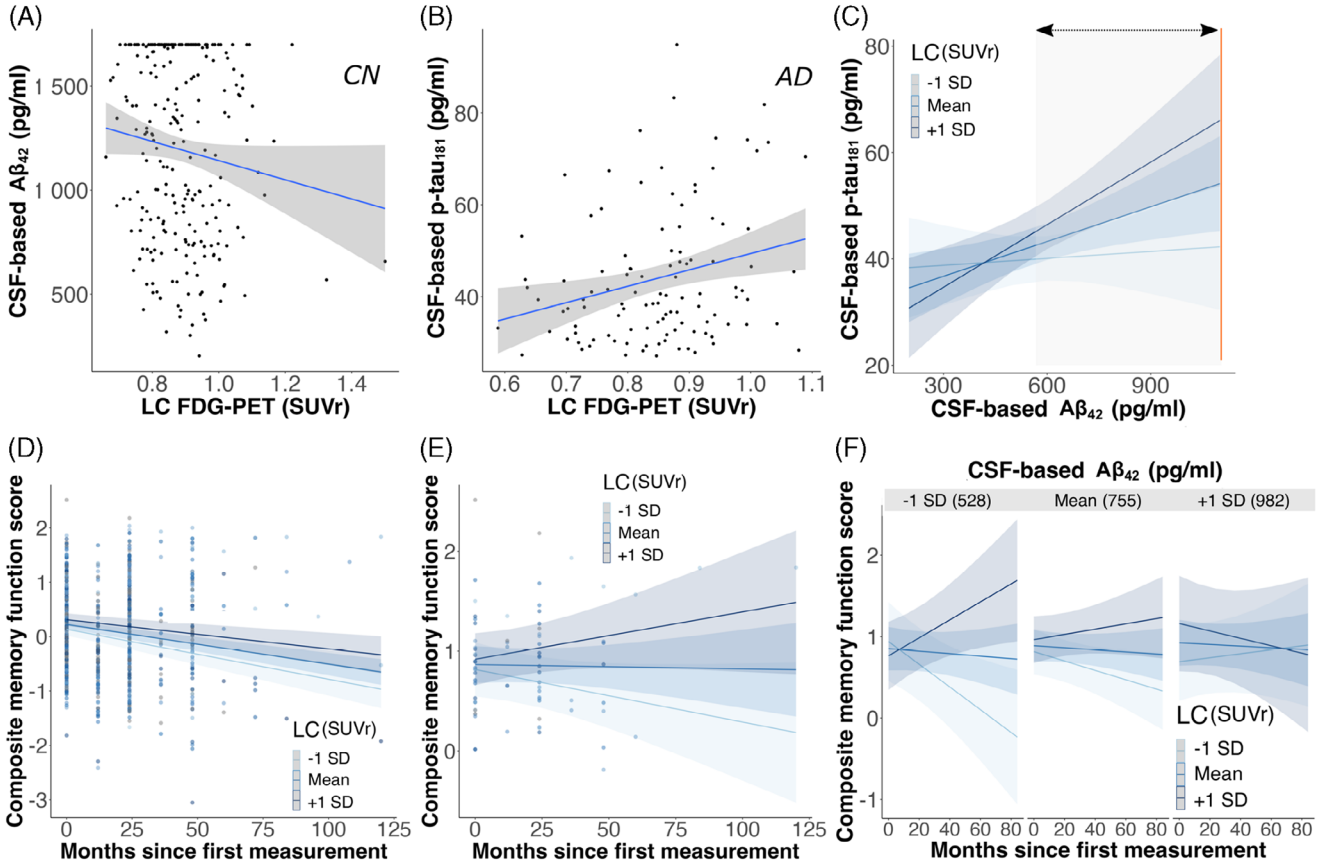

FIGURE 3 Relationships of LC FDG-PET signal and CSF-based biomarkers and memory function. (A) Scatterplot with a regression line and 95% confidence interval shows that lower *CSF-based* Aβ_{42} levels corresponded to higher LC FDG-PET signal in the diagnostic control group. (B) Scatterplot with a regression line and 95% confidence intervals show that higher CSF-based p-tau$_{181}$ levels corresponded to higher LC FDG-PET signal in the AD group. (C) Interaction plot with regression lines and 95% confidence intervals showing that the association of LC FDG-PET signal and CSF-based p-tau varies with different levels of CSF-based Aβ in those with AD. Johnson–Neyman analysis indicated that the relationship between LC FDG-PET signal and CSF-based p-tau$_{181}$ levels is significant for CSF-based Aβ_{42} levels between 576 and 1099 pg/mL, indicated by the gray shaded area and the black arrow. All values in this plot correspond to amyloid positivity, with the orange line marking the threshold. (D) Interaction plot with data points, regression lines, and 95% confidence intervals demonstrating that lower LC FDG-PET signal was associated with faster composite memory function decline in the entire sample. (E) Interaction plot with data points, regression lines, and 95% confidence intervals for the early preclinical group (CN A+T-) shows that memory performance over time was preserved for those with higher LC FDG-PET signal at baseline but declined for those with lower LC FDG-PET signal. (F) Three-way interaction plot with regression lines and 95% confidence intervals for the association of LC FDG-PET signal and composite memory scores over time at specific Aβ levels in the early preclinical group (CN A+T-). Memory decline was steeper in those with lower LC FDG-PET signal, in particular in those with high amyloid burden, whereas high LC FDG-PET signal appears to have a protective effect on memory, even in the presence of high amyloid burden. AB, CSF-based Aβ_{42}; AD, Alzheimer's disease; CN, cognitively normal; CSF, cerebrospinal fluid; FDG-PET, [18F]fluorodeoxyglucose positron emission tomography; LC, locus coeruleus; SUVr, standardized uptake values referenced to the cerebellar white.

3.3 | LC metabolism and CSF-based Aβ and phosphorylated tau

We detected no significant association between LC FDG-PET signal and CSF-based Aβ_{42} (β = 0.000004, *t(597)* = 0.34, p = 0.731) or p-tau$_{181}$ (β = −0.0005, *t*(597) = −0.16, p = 0.871) across the entire sample, adjusted for age and sex. However, when we investigated this relationship within the three diagnostic groups, lower CSF-based Aβ_{42} was associated with higher LC FDG-PET signal in the control group (robust regression: β = −0.00004, *t(236)* = −2.24, p = 0.025, Figure 3A), but there was no association with p-tau$_{181}$ (β = −0.0004, *t(236)* = −0.39, p = 0.698). Linear regression excluding outliers (n = 3) confirmed these results. In the MCI group, there were no significant associations between LC FDG-PET signal and CSF-based Aβ_{42} (β = 0.00002, *t(247)* = 0.57, p = 0.570) or p-tau$_{181}$ (β = 0.0005, *t(247)* = 1.12, p = 0.264). In the AD group, a higher LC FDG-PET signal was associated with higher p-tau values (β = 0.0015, *t(106)* = 2.19, p = 0.031; Figure 3B), but there was no association with CSF Aβ_{42} (β = 0.00002, *t(106)* = −0.29, p = 0.770). Since all AD participants were positive for both tau and Aβ, we performed follow-up interaction analyses with Aβ to examine if the associations between LC FDG-PET and p-tau in the AD group were facilitated by Aβ. The results indicated that individuals with Aβ values closer to the threshold (< 1100 pg/mL), and higher LC metabolism had higher p-tau$_{181}$ values (β = 0.158,

$t(104) = 2.19$, $p = 0.0306$; Figure 3C). A Johnson–Neyman analysis indicated that this relationship was significant for those with CSF-based Aβ levels in the upper range in the AD group (576–1099 pg/mL).

To better understand this counterintuitive relationship, we post hoc examined the relationship between CSF-based Aβ_{42} and p-tau$_{181}$ within the three clinical groups (Figure S3). Lower CSF Aβ_{42} correlated with lower p-tau$_{181}$ levels in the AD group ($r = 0.27$, $p = 0.0035$), but within the CN and MCI groups, lower CSF-based Aβ_{42} correlated with higher p-tau$_{181}$ levels (CN: $r = -0.18$, $p = 0.005$; MCI: $r = -0.105$, $p = 0.09$).

For the disease staging groups, there were no significant associations between LC FDG-PET signal and CSF-based Aβ_{42} or p-tau$_{181}$ respectively within the control ($\beta = 0.00003$, $t(131) = 0.55$, $p = 0.585$; $\beta = 0.0003$, $t(131) = 0.134$, $p = 0.894$), preclinical ($\beta = 0.00006$, $t(101) = -1.08$, $p = 0.284$; $\beta = -0.0015$, $t(101) = -1.28$, $p = 0.204$), and prodromal/AD ($\beta = 0.00002$, $t(357) = 0.75$, $p = 0.454$; $\beta = 0.0005$, $t(357) = 1.45$, $p = 0.148$) groups.

3.4 | LC metabolism and cognition

Lower LC metabolism was related to lower mPACC performance at baseline in the entire sample ($\beta = 7.90$, $t(596) = 3.40$, $p = 0.0007$**), adjusted for age, sex, and years of education. There were no significant interactions with p-tau$_{181}$ ($\beta = 0.04$, $t(594) = 0.32$, $p = 0.75$) or Aβ ($\beta = -0.006$, $t(594) = -1.32$, $p = 0.188$). Further investigation of this relationship within the diagnostic groups showed that this positive association between mPACC and LC FDG-PET signal was only present in the CN group ($\beta = 3.10$, $t(235) = 2.17$, $p = 0.031$*), not in the MCI ($\beta = 2.66$, $t(246) = 1.15$, $p = 0.251$) or AD groups ($\beta = 1.57$, $t(105) = 0.52$, $p = 0.607$; Table S3). For the disease staging groups, there was a significant association between LC FDG-PET signal and mPACC scores for the preclinical group ($\beta = 4.93$, $t(100) = 2.25$, $p = 0.027$*), with higher LC FDG-PET signal corresponding to better mPACC scores. There were no significant associations for the control or prodromal/AD group (control: $\beta = 1.82$, $t(130) = 0.94$, $p = 0.349$; prodromal/AD: $\beta = 4.07$, $t(356) = 1.58$, $p = 0.115$).

In the entire sample, lower LC metabolism was associated with lower scores on the harmonized composite memory score ($\beta = 0.77$, $t(596) = 2.85$, $p = 0.005$**) and lower scores on the harmonized composite executive function score ($\beta = 0.63$, $t(595) = 2.71$, $p = 0.007$**) at baseline. No within-group associations were found between the harmonized domain-specific composite scores at baseline and LC FDG-PET signal for the three diagnostic (CN, MCI, AD) or three disease stages (control, preclinical, prodromal/AD groups (Table S3).

Linear mixed effects models revealed that, in the entire sample, lower LC FDG-PET signal at baseline was associated with faster decline on specifically the harmonized composite memory score ($\beta = 0.016$, $t(279) = 2.23$, $p = 0.027$*; Figure 3D; Table 2). LC FDG-PET signal was not associated with changes in the mPACC digit score ($\beta = 0.095$, $t(273) = 1.04$, $p = 0.298$) or the harmonized composite executive function score ($\beta = 0.002$, $t(272) = 0.21$, $p = 0.831$). We found no evidence that the LC-FDG signal associations with change in memory scores differed between the diagnostic ($\beta = 0.117$, $F(2,339) = 1.21$, $p = 0.298$) or disease stage groups ($\beta = 0.057$, $F(2,306) = 0.80$, $p = 0.451$). In addition, we also found no within-group associations of LC FDG-PET signal at baseline and mPACC digit or harmonized composite scores over time for either the diagnostic or disease staging groups (Table S4). We further explored the associations between LC FDG-PET signal and composite memory scores.

TABLE 2 Statistics for linear mixed-effects models investigating the effect of LC-derived FDG-PET metabolism on cognition over time.

	LC dilated Keren mask			
	β	*T*	*df*	*p*
Cognition				
mPACC digit	0.095	1.04	273	0.298
Composite Memory Function	0.016	2.23	279	0.027*
Composite Executive Function	0.002	0.21	272	0.831

Note: This analysis includes the modified mPACC digit and the harmonized composite scores of the Phenotype Harmonization Consortium (Alzheimer's Disease Sequencing Project [ADSP]) for the memory and executive function subscales. Analyses were adjusted for the covariates of age, sex, and years of education.
Abbreviation: mPACC, Preclinical Alzheimer's Cognitive Composite.
*Indicates the *p*-value was below the critical value determined with the Benjamini–Hochberg adaptive step-up FDR correction procedure at $q = 0.1$.

As we previously observed that higher LC FDG-PET signal was associated with lower CSF Aβ_{42} but not with higher CSF p-tau^{181} in the cognitively unimpaired group (Figure 3A), we aimed to understand the functional interpretation of this relationship by post hoc examining the relationship between LC FDG-PET signal, composite memory scores, and Aβ_{42} in the early preclinical AD group with below threshold CSF-based Aβ_{42} (CN A+T-). Linear mixed effects models showed that in the early preclinical AD group, higher LC FDG-PET signal at baseline was associated with slower decline on the composite memory score ($\beta = 0.036$, $t(37) = 2.11$, $p = 0.041$; Figure 3E), which marginally depended on the level of CSF Aβ_{42} as indicated by a three-way interaction of LC FDG-PET signal * time * Aβ_{42} (SS = 0.14, $F(1,23) = 3.897$, $p = 0.06$; Figure 3F). Lower LC metabolism corresponded to worse memory performance over time at lower CSF Aβ_{42} values (< ~725 pg/mL), whereas those with higher LC metabolism showed attenuated memory decline. CSF Aβ_{42} levels on their own are not associated with memory performance over time in the early preclinical AD group (CN A+T-; $\beta = -0.000007$, $t(20) = -0.07$, $p = 0.943$). In contrast, among those with no cognitive impairment and Aβ_{42} and p-tau$_{181}$ positivity (CN A+T+), the LC FDG-PET signal was not associated with memory performance over time ($\beta = -0.03$, $t(5) = -0.51$, $p = 0.635$), also not in interaction with CSF Aβ_{42} ($SS = 0.05$, $F(1,6) = 0.73$, $p = 0.425$), nor was this the case for the group with cognitive impairment and Aβ positivity ($\beta = 0.006$, $t(172) = 0.66$, $p = 0.508$), also not in interaction with CSF Aβ_{42} levels ($SS = 0.053$, $F(1,184) = 1.59$, $p = 0.208$).

We performed post hoc analyses to verify our findings on the association between LC FDG signal and harmonized composite memory scores over time by restricting our analyses to the first 24 months, which is the timeframe during which the majority of data points

were collected. This replicated our findings of the LC FDG-PET signal by time interaction on memory function for the entire group ($\beta = 0.019$, $t(259) = 2.29$, $p = 0.023$) and the preclinical group ($\beta = 0.032$, $t(24) = 2.23$, $p = 0.035$). Since some time points had sparse data, we additionally ran a linear mixed effects model including time points with $n > 5$ data points, resulting in similar findings for the entire group ($\beta = 0.016$, $t(281) = 2.24$, $p = 0.026$) and the preclinical group ($\beta = 0.036$ $t(36) = 2.05$, $p = 0.048$). This suggests that our findings are not driven by the time points with sparser data.

3.5 | Control and sensitivity analyses

We repeated the analyses performed with the LC using the isthmus of the cingulate. Older individuals had lower isthmus FDG-PET signals ($\beta = -0.0074$, $t(601) = -6.00$, $p < 0.0001$; Figure S4A), as did females ($\beta = -0.0413$, $t(601) = -2.33$, $p = 0.020$; Figure S4B). LC and isthmus FDG-PET values are associated, with higher LC values corresponding to higher isthmus values ($\beta = 0.3768$, $t(597) = 4.95$, $p < 0.0001$; Figure S4C). Clinical diagnosis was associated with isthmus FDG-PET signal ($F(2,598) = 101.86$, $p < 0.0001$; Figure S4D), with lower values in the MCI ($\beta = -0.1337$, $t = -8.11$, $p < 0.0001$) and AD groups ($\beta = -0.2937$, $t = -14.01$, $p < 0.0001$) compared to the CN group. Disease staging was negatively associated with isthmus FDG-PET signal ($F(2,598) = 67.95$, $p < 0.0001$), which was more pronounced in the A+T+ groups compared to the A+T- groups (Figure S4E). Furthermore, lower isthmus FGD-PET signal was associated with higher CSF-based p-tau$_{181}$ ($\beta = -0.004$, $t(599) = -7.88$, $p < 0.0001$; S4F), lower Aβ_{42} values ($\beta = 0.0002$, $t(599) = 10.15$, $p < 0.0001$; Figure S4G), and worse mPACC scores ($\beta = 17.25$, $t(599) = 16.37$, $p < 0.0001$; Figure S4H).

Sensitivity analyses using a shifted LC mask resulted in non-significant findings for the relationships between LC metabolism and age, sex, CSF-based p-tau$_{181}$, CSF-based Aβ_{42}, diagnostic and disease staging groups, and mPACC scores, but did show a significant positive association with years of education (Table S5). Extracting LC FDG-PET signal from the non-deblurred or joint-entropy prior corrected images resulted in non-significant associations between LC metabolism and diagnostic ($F(2,597) = 0.65$, $p = 0.524$) or disease stage groups ($F(2,597) = 1.84$, $p = 0.160$), replicating previously reported findings[39] (Figure S5). Our reported standardized uptake value referenced to the cerebellar white (SUVr) values are similar to these previously reported findings. We further repeated our analysis with the 7T-derived LC mask (Figure S1) and performed the same analyses using the pons, excluding the LC, as reference region (Table S6). Results were similar to the primary mask and the CW reference region (dilated and smoothed Keren mask, referenced to CW) for the association of LC-derived FDG-PET signal and age, CSF values, disease stage grouping, and mPACC scores. However, the pons-referenced analyses did not show significant differences between the diagnostic groups. Furthermore, the 7T LC masks did not show significant sex differences, while the LC-derived FDG-PET signal using the dilated and smoothed Keren mask showed lower LC-derived FDG-PET signal in males. We further repeated the analyses of the FDG-PET signal * time * amyloid interaction on memory scores for the isthmus signal ($\beta = -0.00001$, $t(33) = -0.12$, $p = 0.903$) and the LC signal extracted from the non-deblurred FDG scans ($\beta = -0.0004$, $t(25) = -1.66$, $p = 0.109$) (Figure S6).

4 | DISCUSSION

Recognition that the accumulation of neuropathologic hallmarks of AD starts decades before the emergence of clinical symptoms has reinforced the need for an early marker of AD-related changes. Autopsy and imaging studies suggest the noradrenergic LC, one of the first regions to accumulate tau pathology early in adulthood, as a promising early marker.[1–7,23,40] The altered metabolic activity of the LC, implied by elevated levels of NE-metabolites, has been suggested to reflect compensatory mechanisms but has also been associated with greater tau deposition during disease progression.[13,14] In later disease stages, waning LC metabolism has been hypothesized to correspond to local neuronal atrophy and cell death. Guided by these findings, we investigated whether LC metabolism varies nonlinearly with disease stage, with elevated metabolism in the earliest stages and lower metabolism in the later stages. We further investigated the functional implications of these metabolic levels across disease stages by combining LC-derived FDG-PET signal with CSF-based Aβ_{42}, p-tau$_{181}$, and serial cognitive measurements. Here, we demonstrated that LC metabolism is higher in the earliest preclinical stages, in the presence of elevated Aβ_{42}, whereas LC metabolism is lower when elevated tau and cognitive impairment are also present. Interestingly, this elevated metabolism in the early preclinical stage was associated with attenuated memory decline, indicating that higher LC metabolism may confer cognitive resilience in the face of amyloid pathology early in the disease. Whether cognitive resilience provided by higher LC FDG signal may ultimately lead to faster disease progression when these compensational resources are depleted remains unknown. We do see higher LC metabolism associated with elevated CSF p-tau$_{181}$ in AD patients, particularly in individuals in the earlier stages of Aβ_{42} positivity, possibly signaling detrimental processes.

In alignment with the hypothesized nonlinear metabolic pattern,[22] we observed higher LC metabolism in the preclinical AD group compared to both the asymptomatic biomarker-negative and cognitively impaired biomarker-positive groups. Our findings demonstrate that these elevations in LC metabolism covary with Aβ positivity and not tau in the preclinical group. Autopsy studies have reported early involvement of tau in the LC, but the role of Aβ in LC physiology in the earliest stages of the disease remains unknown. As such, lower LC metabolism in the A+T+ preclinical AD group may capture individuals who progressed further on the disease trajectory than the A+T- group. In line with our expectations, we observed lower LC metabolism in the AD group.

CSF measures of Aβ capture soluble and fibrillar forms of Aβ, resulting in earlier detection of amyloid than PET measures, and are more likely to reflect the earliest stages of amyloid accumulation in

the preclinical trajectory.[41–45] Amyloid oligomers may play a role in tau phosphorylation pathways[46] and are presumably more toxic than fibrillar forms,[47–50] but the role of the LC-NE system in amyloid aggregation or amyloid-related tauopathy in asymptomatic individuals with CSF-based $A\beta_{42}$ positivity remains underexplored.[51] Animal studies suggested that Aβ oligomers can hijack the alpha2-adrenergic receptors, initiating a GSK3/ß pathway of tau hyperphosphorylation.[52] It remains unknown whether Aβ oligomers are present in the LC in the earliest stages of the disease and whether this impacts the metabolism of LC neurons. Human AD *post mortem* tissue and animal work showed Aβ oligomer expression in the LC, which was accompanied by a reduction of GABA-A receptors, resulting in LC neuronal hyperexcitability in the APP-PSEN1 mouse model.[53] Higher glucose availability in the LC may provide an environment that keeps this cycle of hyperexcitability going, as in-vitro data suggest that glucose molecules in the extracellular space facilitate $A\beta_{42}$ oligomer formation.[54]

The observed heightened LC metabolism concomitant with the emergence of AD pathology, which dwindles as the disease progresses, suggests that LC metabolism is dynamic during the disease and may contribute to its unique vulnerability. Interestingly, we observed that higher LC metabolism in the preclinical AD group was associated with better memory performance over time, particularly in those with lower levels of CSF-based $A\beta_{42}$. In contrast, those with lower LC metabolism performed worse over time in the presence of low levels of CSF $A\beta_{42}$. We did not find these associations with memory in the prodromal/AD group. These findings suggest that elevated metabolism in the early asymptomatic stages may provide a certain degree of protection from the detrimental effect of Aβ on memory but may no longer be able to rescue the detrimental effects of widespread pathology and neurodegeneration in later stages of the disease.

Such a protective effect is consistent with recent PET studies examining catecholamine synthesis in the LC, reporting lower tau pathology and attenuated memory decline in the preclinical AD group with higher LC catecholamine synthesis.[20,21] However, in AD patients, where we identified a positive association between LC metabolism and p-tau_{181}, increases in CSF MHPG have been associated with higher levels of AD pathology, cortical atrophy, faster cognitive decline, and higher levels of neuropsychiatric symptoms,[13] suggesting that in later disease stages, higher NE metabolic turnover may be detrimental or accompanies detrimental processes. CSF studies do not provide spatially specific information and likely capture NE-metabolism in the projection areas of the LC, which may be influenced by dysregulation of the enzymes breaking down NE (COMT, MAO), impaired negative feedback signaling of adrenergic receptors or impaired reuptake by NE transporters. However, *post mortem* findings also provided evidence for the upregulation of NE synthesis concomitant with larger degrees of neuronal loss.[55] Even with upregulated NE synthesis and release, local neuronal atrophy and cell death in the LC in later disease stages may contribute to the waning LC metabolism measured with FDG-PET, which reflects the metabolism of the entire region. We did not examine subparts of the LC, but distinct subpopulations of LC neurons may be selectively vulnerable to pathology.[31] Recent studies recognized the heterogeneity in the synaptic and functional architecture of the LC, with distinct populations targeting projection areas that are differently involved in cognitive processes.[56,57]

When comparing previous studies to our results, we recognize the differences in sensitivity and biological correlates, given that FDG-PET measures glucose uptake in neurons and astrocytes. Previous work has shown that the FDG-PET signal is substantially affected by the alteration of astroglial glutamate transport,[58,59] and astrocyte reactivity plays a role as an upstream modulator in the coupling of Aβ and initial phosphorylated tau in preclinical AD.[60] There is a coupling between NE release and glucose metabolism, as NE upregulates the expression of monocarboxylate transporters (MCT2) on neuronal membranes,[61] which allows neurons to take up astrocyte-derived lactate,[62–64] which is synthesized via glycolysis triggered by NE release.[63,65,66] This indicates that changes in LC FDG-PET signal can reflect neural synaptic dysfunction and astrocyte reactivity.

The LC has been implicated in memory and learning,[67,68] most likely because of the role NE plays in long-term potentiation.[69,70] We observed that higher LC metabolism was associated with better memory performance in the entire group, both at baseline and longitudinally. Lower LC metabolism specifically predicted memory decline but not changes in global cognition or executive functions. Our results are in line with reports on the selective involvement of the LC pathway in memory processes,[71,72] with better structural integrity and functional activity having a memory-promoting effect.[23,24,73]

The current study has limitations. Although our findings are promising and consistent with the existing literature, we did not correct for multiple comparisons except for direct group comparisons and cognition. However, we performed several sensitivity and control analyses to demonstrate the robustness of our findings. First, we replicated previously established group differences in the FDG-PET signal of the posterior cingulate's isthmus.[33,34] Then, we replicated previous work reporting no differences in non-deblurred LC FDG-signal between diagnostic groups,[39] indicating that deblurring and partial-volume correction are essential when studying small structures like the LC with techniques that lack high spatial resolution. Finally, by shifting the LC more ventrally, we were able to demonstrate the specificity of our findings. While these findings demonstrate promising in-vivo associations of LC metabolism with AD phenotypes, replication and validation in other cohorts are crucial. Furthermore, the field still lacks spatially specific measures to investigate in-vivo tau accumulation in the LC, as most tau-PET ligands bind to neuromelanin in the LC and nearby choroid plexus, confounding any information on tau. Therefore, we cannot examine the effect of local tau on the metabolic changes we observed across diagnostic and disease stage groups. CSF-based p-tau measures likely predominantly reflect cortical tau accumulation since cortical regions have considerably larger cell counts with the potential of producing and releasing hyperphosphorylated tau. Therefore, the CSF p-tau measures may give limited information about tau originating from the LC, and we cannot separate the LC contributions to the CSF p-tau signal from cortical contributions.

5 | CONCLUSION

In summary, FDG-PET-derived LC metabolism is associated with diagnostic status and higher LC metabolism was observed in the preclinical stages, followed by lower LC metabolism in the later stages of the disease. In the preclinical stages, higher LC metabolism provided resilience against memory decline, particularly in the presence of a higher amyloid burden. In AD patients, higher LC metabolism correlated with greater CSF p-tau$_{181}$ in the earlier stages of amyloid accumulation but was not directly associated with preserved cognition as individuals have dementia, possibly signaling detrimental processes. These in-vivo and spatially specific findings suggest that metabolism of the LC, as measured with FDG-PET signal, is upregulated in the early preclinical stages of AD, making it of interest to future research elucidating the mechanisms underlying vulnerability to pathology emergence and can inform studies developing early interventions supporting the LC pathway to potentially modify the trajectory of cognitive decline.

ACKNOWLEDGMENTS

Data collection and sharing for this project was funded by the Alzheimer's Disease Neuroimaging Initiative (ADNI) (National Institutes of Health Grant U01 AG024904) and DOD ADNI (Department of Defense award number W81XWH-12-2-0012). ADNI is funded by the National Institute on Aging, the National Institute of Biomedical Imaging and Bioengineering, and through generous contributions from the following: AbbVie, Alzheimer's Association; Alzheimer's Drug Discovery Foundation; Araclon Biotech; BioClinica, Inc.; Biogen; Bristol-Myers Squibb Company; CereSpir, Inc.; Cogstate; Eisai Inc.; Elan Pharmaceuticals, Inc.; Eli Lilly and Company; EuroImmun; F. Hoffmann-La Roche Ltd and its affiliated company Genentech, Inc.; Fujirebio; GE Healthcare; IXICO Ltd.;Janssen Alzheimer Immunotherapy Research & Development, LLC.; Johnson & Johnson Pharmaceutical Research & Development LLC.; Lumosity; Lundbeck; Merck & Co., Inc.;Meso Scale Diagnostics, LLC.; NeuroRx Research; Neurotrack Technologies; Novartis Pharmaceuticals Corporation; Pfizer Inc.; Piramal Imaging; Servier; Takeda Pharmaceutical Company; and Transition Therapeutics. The Canadian Institutes of Health Research is providing funds to support ADNI clinical sites in Canada. Private sector contributions are facilitated by the Foundation for the National Institutes of Health (www.fnih.org). The grantee organization is the Northern California Institute for Research and Education, and the study is coordinated by the Alzheimer's Therapeutic Research Institute at the University of Southern California. ADNI data are disseminated by the Laboratory for Neuro Imaging at the University of Southern California. This work was supported by an Alzheimer's Association Research Fellowship (Koops, 23AARF-1026796) and by funding from the National Institutes of Health (Jacobs, R21 AG074220). This research was carried out in part at the Athinoula A. Martinos Center for Biomedical Imaging at the Massachusetts General Hospital, using resources provided by the Center for Functional Neuroimaging Technologies, P41EB015896, a P41 Biotechnology Resource Grants supported by the National Institute of Biomedical Imaging and Bioengineering (NIBIB), National Institutes of Health. This work also involved the use of instrumentation supported by the NIH Shared Instrumentation Grant Program and/or High-End Instrumentation Grant Program, grant numbers S10RR023401 and S10RR023043.

CONFLICT OF INTEREST STATEMENT

The authors report no relevant conflicts of interest. E.A.K., J.D., J.A.B., M.V.E., P.C.P., J.C.P., H.I.L.J. have no disclosures. B.J.H. has served as paid consultant for Biogen, Eisai, and Roche. R.A.S. has served as a paid consultant for AbbVie, AC Immune, Acumen, Alector, Biohaven, Genentech, Ionis, Janssen, Prothena, and Roche. She has received research support for public-private clinical trials Eisai and Eli Lilly. K.A.J. has served as a paid consultant for Janssen, Merck, Prothena, and Novartis, and has served as a site co-investigator for Lilly, Eisai, Janssen, Cerveau, and Biogen. These relationships are not related to the content of this manuscript. Author disclosures are available in the Supporting Information.

CONSENT STATEMENT

All human subjects included in the ADNI database provided informed consent.

ORCID

Elouise A. Koops https://orcid.org/0000-0002-4105-4254

REFERENCES

1. Braak H, Thal DR, Ghebremedhin E, Del Tredici K. Stages of the pathologic process in Alzheimer disease: age categories from 1 to 100 years. *J Neuropathol Exp Neurol*. 2011;70(11):960-969.
2. Braak H, Braak E. Neuropathological stageing of Alzheimer-related changes. *Acta Neuropathol*. 1991;82(4):239-259.
3. Ehrenberg AJ, Nguy AK, Theofilas P, et al. Quantifying the accretion of hyperphosphorylated tau in the locus coeruleus and dorsal raphe nucleus: the pathological building blocks of early Alzheimer's disease. *Neuropathol Appl Neurobiol*. 2017;43(5):393-408.
4. Gilvesy A, Husen E, Magloczky Z, et al. Spatiotemporal characterization of cellular tau pathology in the human locus coeruleus-pericoerulear complex by three-dimensional imaging. *Acta Neuropathol*. 2022;144(4):651-676.
5. Theofilas P, Ehrenberg AJ, Dunlop S, et al. Locus coeruleus volume and cell population changes during Alzheimer's disease progression: a stereological study in human postmortem brains with potential implication for early-stage biomarker discovery. *Alzheimers Dement*. 2017;13(3):236-246.
6. Kelly SC, He B, Perez SE, Ginsberg SD, Mufson EJ, Counts SE. Locus coeruleus cellular and molecular pathology during the progression of Alzheimer's disease. *Acta Neuropathol Commun*. 2017;5(1):8.
7. German DC, Manaye KF. Disease-specific patterns of locus coeruleus cell loss. *Ann Neurol*. 1992;32(5):667-676.
8. Dubois B, Hampel H, Feldman HH, et al. Preclinical Alzheimer's disease: definition, natural history, and diagnostic criteria. *Alzheimers Dement*. 2016;12(3):292-323.
9. Lecas JC. Locus coeruleus activation shortens synaptic drive while decreasing spike latency and jitter in sensorimotor cortex. Implications for neuronal integration. *Eur J Neurosci*. 2004;19(9):2519-2530.
10. Atzori M, Cuevas-Olguin R, Esquivel-Rendon E, et al. Locus ceruleus norepinephrine release: a central regulator of CNS spatio-temporal activation? *Front Synaptic Neurosci*. 2016;8:25.

11. Magistretti PJ, Morrison JH. Noradrenaline- and vasoactive intestinal peptide-containing neuronal systems in neocortex: functional convergence with contrasting morphology. *Neuroscience*. 1988;24(2):367-378.
12. Magistretti PJ, Sorg O, Yu N, Martin JL, Pellerin L. Neurotransmitters regulate energy metabolism in astrocytes: implications for the metabolic trafficking between neural cells. *Dev Neurosci*. 1993;15(3-5):306-312.
13. Jacobs HIL, Riphagen JM, Ramakers I, Verhey FRJ. Alzheimer's disease pathology: pathways between central norepinephrine activity, memory, and neuropsychiatric symptoms. *Mol Psychiatry*. 2021;26(3):897-906.
14. Kang SS, Liu X, Ahn EH, et al. Norepinephrine metabolite DOPEGAL activates AEP and pathological Tau aggregation in locus coeruleus. *J Clin Invest*. 2020;130(1):422-437.
15. Raskind MA, Peskind ER, Holmes C, Goldstein DS. Patterns of cerebrospinal fluid catechols support increased central noradrenergic responsiveness in aging and Alzheimer's disease. *Biol Psychiatry*. 1999;46(6):756-765.
16. Sheline YI, Miller K, Bardgett ME, Csernansky JG. Higher cerebrospinal fluid MHPG in subjects with dementia of the Alzheimer type. Relationship with cognitive dysfunction. *Am J Geriatr Psychiatry*. 1998;6(2):155-161.
17. Lawlor BA, Bierer LM, Ryan TM, et al. Plasma 3-Methoxy-4-Hydroxyphenylglycol (MHPG) and clinical symptoms in Alzheimer's disease. *Biol Psychiatry*. 1995;38(3):185-188.
18. Raskind MA, Peskind ER, Halter JB, Jimerson DC. Norepinephrine and MHPG levels in CSF and plasma in Alzheimer's disease. *Arch Gen Psychiatry*. 1984;41(4):343-346.
19. Henjum K, Watne LO, Godang K, et al. Cerebrospinal fluid catecholamines in Alzheimer's disease patients with and without biological disease. *Transl Psychiatry*. 2022;12(1):151.
20. Ciampa CJ, Parent JH, Harrison TM, et al. Associations among locus coeruleus catecholamines, tau pathology, and memory in aging. *Neuropsychopharmacology*. 2022;47(5):1106-1113.
21. Parent JH, Ciampa CJ, Harrison TM, et al. Locus coeruleus catecholamines link neuroticism and vulnerability to tau pathology in aging. *Neuroimage*. 2022;263:119658.
22. Weinshenker D. Long road to ruin: noradrenergic dysfunction in neurodegenerative disease. *Trends Neurosci*. 2018;41(4):211-223.
23. Jacobs HIL, Becker JA, Kwong K, et al. In vivo and neuropathology data support locus coeruleus integrity as indicator of Alzheimer's disease pathology and cognitive decline. *Sci Transl Med*. 2021;13(612):eabj2511.
24. Prokopiou PC, Engels-Domínguez N, Papp KV, et al. Lower novelty-related locus coeruleus function is associated with Aβ-related cognitive decline in clinically healthy individuals. *Nat Commun*. 2022;13(1):1571.
25. Dienel GA. Brain glucose metabolism: integration of energetics with function. *Physiol Rev*. 2019;99(1):949-1045.
26. Song TA, Yang F, Chowdhury SR, et al. PET image deblurring and super-resolution with an MR-based joint entropy prior. *IEEE Trans Comput Imaging*. 2019;5(4):530-539.
27. Jack CR Jr, Bennett DA, Blennow K, et al. NIA-AA Research Framework: toward a biological definition of Alzheimer's disease. *Alzheimers Dement*. 2018;14(4):535-562.
28. Dale AM, Fischl B, Sereno MI. Cortical surface-based analysis. I. Segmentation and surface reconstruction. *Neuroimage*. 1999;9(2):179-194.
29. Iglesias JE, Van Leemput K, Bhatt P, et al; Alzheimer's Disease Neuroimaging I. Bayesian segmentation of brainstem structures in MRI. *Neuroimage*. 2015;113:184-195.
30. Klein A, Andersson J, Ardekani BA, et al. Evaluation of 14 nonlinear deformation algorithms applied to human brain MRI registration. *Neuroimage*. 2009;46(3):786-802.
31. Van Egroo M, Riphagen JM, Ashton NJ, et al. Ultra-high field imaging, plasma markers and autopsy data uncover a specific rostral locus coeruleus vulnerability to hyperphosphorylated tau. *Mol Psychiatry*. 2023;28(6):2412-2422.
32. Keren NI, Lozar CT, Harris KC, Morgan PS, Eckert MA. In vivo mapping of the human locus coeruleus. *Neuroimage*. 2009;47(4):1261-1267.
33. Baran TM, Lin FV, Alzheimer's Disease Neuroimaging I. Amyloid and FDG PET of successful cognitive aging: global and cingulate-specific differences. *J Alzheimers Dis*. 2018;66(1):307-318.
34. Strom A, Iaccarino L, Edwards L, et al. Cortical hypometabolism reflects local atrophy and tau pathology in symptomatic Alzheimer's disease. *Brain*. 2022;145(2):713-728.
35. McKay NS, Gordon BA, Hornbeck RC, et al. Positron emission tomography and magnetic resonance imaging methods and datasets within the Dominantly Inherited Alzheimer Network (DIAN). *Nat Neurosci*. 2023;26(8):1449-1460.
36. Mukherjee S, Choi SE, Lee ML, et al. Cognitive domain harmonization and cocalibration in studies of older adults. *Neuropsychology*. 2023;37(4):409-423.
37. Benjamini Y, Hochberg Y. Controlling the false discovery rate: a practical and powerful approach to multiple testing. *J R Stat Soc*. 1995;57(1):289-300.
38. Benjamini Y, Hochberg Y. On the adaptive control of the false discovery rate in multiple testing with independent statistics. *J Educ Behav Stat*. 2000;25(1):60-83.
39. Liu KY, Acosta-Cabronero J, Hong YT, et al.; Alzheimer's Disease Neuroimaging I. FDG-PET assessment of the locus coeruleus in Alzheimer's disease. *Neuroimage Rep*. 2021;1(1):100002.
40. Betts MJ, Kirilina E, Otaduy MCG, et al. Locus coeruleus imaging as a biomarker for noradrenergic dysfunction in neurodegenerative diseases. *Brain*. 2019;142(9):2558-2571.
41. Vlassenko AG, McCue L, Jasielec MS, et al. Imaging and cerebrospinal fluid biomarkers in early preclinical alzheimer disease. *Ann Neurol*. 2016;80(3):379-387.
42. Fagan AM, Head D, Shah AR, et al. Decreased cerebrospinal fluid Abeta(42) correlates with brain atrophy in cognitively normal elderly. *Ann Neurol*. 2009;65(2):176-183.
43. Hoglund K, Kern S, Zettergren A, et al. Preclinical amyloid pathology biomarker positivity: effects on tau pathology and neurodegeneration. *Transl Psychiatry*. 2017;7(1):e995.
44. Skoog I, Davidsson P, Aevarsson O, Vanderstichele H, Vanmechelen E, Blennow K. Cerebrospinal fluid beta-amyloid 42 is reduced before the onset of sporadic dementia: a population-based study in 85-year-olds. *Dement Geriatr Cogn Disord*. 2003;15(3):169-176.
45. Jansen WJ, Ossenkoppele R, Knol DL, et al. Prevalence of cerebral amyloid pathology in persons without dementia: a meta-analysis. *JAMA*. 2015;313(19):1924-1938.
46. Ma QL, Yang F, Rosario ER, et al. Beta-amyloid oligomers induce phosphorylation of tau and inactivation of insulin receptor substrate via c-Jun N-terminal kinase signaling: suppression by omega-3 fatty acids and curcumin. *J Neurosci*. 2009;29(28):9078-9089.
47. Shankar GM, Li S, Mehta TH, et al. Amyloid-beta protein dimers isolated directly from Alzheimer's brains impair synaptic plasticity and memory. *Nat Med*. 2008;14(8):837-842.
48. He Y, Zheng MM, Ma Y, et al. Soluble oligomers and fibrillar species of amyloid beta-peptide differentially affect cognitive functions and hippocampal inflammatory response. *Biochem Biophys Res Commun*. 2012;429(3-4):125-130.
49. Nimmrich V, Grimm C, Draguhn A, et al. Amyloid beta oligomers (A beta(1-42) globulomer) suppress spontaneous synaptic activity by inhibition of P/Q-type calcium currents. *J Neurosci*. 2008;28(4):788-797.
50. Zhang Y, Lu L, Jia J, et al. A lifespan observation of a novel mouse model: in vivo evidence supports abeta oligomer hypothesis. *PLoS One*. 2014;9(1):e85885.

51. Matchett BJ, Grinberg LT, Theofilas P, Murray ME. The mechanistic link between selective vulnerability of the locus coeruleus and neurodegeneration in Alzheimer's disease. *Acta Neuropathol*. 2021;141(5):631-650.
52. Zhang F, Gannon M, Chen Y, et al. beta-amyloid redirects norepinephrine signaling to activate the pathogenic GSK3beta/tau cascade. *Sci Transl Med*. 2020;12(526).
53. Kelly L, Seifi M, Ma R, et al. Identification of intraneuronal amyloid beta oligomers in locus coeruleus neurons of Alzheimer's patients and their potential impact on inhibitory neurotransmitter receptors and neuronal excitability. *Neuropathol Appl Neurobiol*. 2021;47(4):488-505.
54. Kedia N, Almisry M, Bieschke J. Glucose directs amyloid-beta into membrane-active oligomers. *Phys Chem Chem Phys*. 2017;19(27):18036-18046.
55. Szot P, White SS, Greenup JL, Leverenz JB, Peskind ER, Raskind MA. Compensatory changes in the noradrenergic nervous system in the locus ceruleus and hippocampus of postmortem subjects with Alzheimer's disease and dementia with Lewy bodies. *J Neurosci*. 2006;26(2):467-478.
56. McKinney A, Hu M, Hoskins A, et al. Cellular composition and circuit organization of the locus coeruleus of adult mice. *Elife*. 2023;12.
57. Ma HT, Zhang HC, Zuo ZF, Liu YX. Heterogeneous organization of Locus coeruleus: an intrinsic mechanism for functional complexity. *Physiol Behav*. 2023;268:114231.
58. Zimmer ER, Parent MJ, Souza DG, et al. [(18)F]FDG PET signal is driven by astroglial glutamate transport. *Nat Neurosci*. 2017;20(3):393-395.
59. Rocha A, Bellaver B, Souza DG, et al. Clozapine induces astrocyte-dependent FDG-PET hypometabolism. *EJNMMI*, 2022;49(7):2251-2264. https://doi.org/10.1007/s00259-022-05682-3
60. Bellaver B, Povala G, Ferreira PCL, et al. Astrocyte reactivity influences amyloid-beta effects on tau pathology in preclinical Alzheimer's disease. *Nat Med*. 2023;29(7):1775-1781.
61. Pierre K, Debernardi R, Magistretti PJ, Pellerin L. Noradrenaline enhances monocarboxylate transporter 2 expression in cultured mouse cortical neurons via a translational regulation. *J Neurochem*. 2003;86(6):1468-1476.
62. Yu N, Martin JL, Stella N, Magistretti PJ. Arachidonic acid stimulates glucose uptake in cerebral cortical astrocytes. *Proc Natl Acad Sci U S A*. 1993;90(9):4042-4046.
63. Sorg O, Magistretti PJ. Characterization of the glycogenolysis elicited by vasoactive intestinal peptide, noradrenaline and adenosine in primary cultures of mouse cerebral cortical astrocytes. *Brain Res*. 1991;563(1-2):227-233.
64. Medel V, Crossley N, Gajardo I, et al. Whole-brain neuronal MCT2 lactate transporter expression links metabolism to human brain structure and function. *Proc Natl Acad Sci U S A*. 2022;119(33):e2204619119.
65. Hertz L, Lovatt D, Goldman SA, Nedergaard M. Adrenoceptors in brain: cellular gene expression and effects on astrocytic metabolism and [Ca(2+)]i. *Neurochem Int*. 2010;57(4):411-420.
66. Coggan JS, Keller D, Cali C, et al. Norepinephrine stimulates glycogenolysis in astrocytes to fuel neurons with lactate. *PLoS Comput Biol*. 2018;14(8):e1006392.
67. James T, Kula B, Choi S, Khan SS, Bekar LK, Smith NA. Locus coeruleus in memory formation and Alzheimer's disease. *Eur J Neurosci*. 2021;54(8):6948-6959.
68. Jacobs HI, Priovoulos N, Poser BA, et al. Dynamic behavior of the locus coeruleus during arousal-related memory processing in a multi-modal 7T fMRI paradigm. *Elife*. 2020;9.
69. Tully K, Bolshakov VY. Emotional enhancement of memory: how norepinephrine enables synaptic plasticity. *Mol Brain*. 2010;3:15.
70. Stanton PK, Sarvey JM. Norepinephrine regulates long-term potentiation of both the population spike and dendritic EPSP in hippocampal dentate gyrus. *Brain Res Bull*. 1987;18(1):115-119.
71. Chowdhury A, Luchetti A, Fernandes G, et al. A locus coeruleus-dorsal CA1 dopaminergic circuit modulates memory linking. *Neuron*. 2022;110(20):3374-3388. e8.
72. Hammerer D, Callaghan MF, Hopkins A, et al. Locus coeruleus integrity in old age is selectively related to memories linked with salient negative events. *Proc Natl Acad Sci U S A*. 2018;115(9):2228-2233.
73. Dahl MJ, Mather M, Duzel S, et al. Rostral locus coeruleus integrity is associated with better memory performance in older adults. *Nat Hum Behav*. 2019;3(11):1203-1214.

SUPPORTING INFORMATION

Additional supporting information can be found online in the Supporting Information section at the end of this article.

How to cite this article: Koops EA, Dutta J, Hanseeuw BJ, et al.; for the Alzheimer's Disease Neuroimaging Initiative. Elevated locus coeruleus metabolism provides resilience against cognitive decline in preclinical Alzheimer's disease. *Alzheimer's Dement*. 2024;1-14.
https://doi.org/10.1002/alz.14385